

Leafhopper Wing-Inspired Broadband Omnidirectional Antireflective Embroidered Ball-Like Structure Arrays Using a Nonlithography-Based Methodology

Chih-Wei Lei, Ru-Yu Chen, and Hongta Yang*



Cite This: *Langmuir* 2020, 36, 5296–5302



Read Online

ACCESS |



Metrics & More

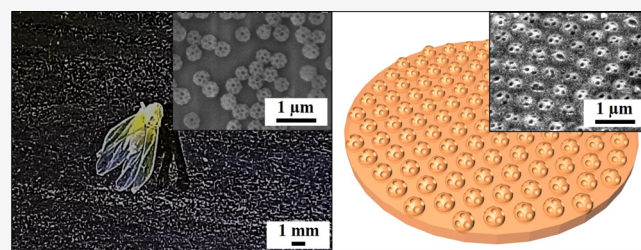


Article Recommendations



Supporting Information

ABSTRACT: Leafhoppers (*Thaia rubiginosa*) actively coat their wings with embroidered ball-like secretory brochosomes, which act as antireflective structures to enhance camouflage against predators. Inspired by the leafhoppers, we report a scalable nonlithographic approach for self-assembling nonclose-packed embroidered ball-like hierarchical structure arrays. The resulting structures create a gradual refractive index transition at the air/substrate interface, thereby suppressing the optical reflection for wide viewing angles. Compared with a bare substrate, the average reflectance of the structured substrate in the whole visible spectral region is reduced from 9 to 3% at normal incidence, and the average reflectance of that is even reduced by ca. 22% as the incident angle reaches 75°. Moreover, the dependence of the height and the shape of the hierarchical structure on the omnidirectional antireflection performance is systemically evaluated in this research.



INTRODUCTION

Optical reflection, also known as Fresnel reflection, occurs when light is incident upon any interface between two media with different refractive indices, and the incidence angle is equal to the reflection angle.^{1,2} The formation of Fresnel reflection, which is dependent upon the mismatched refractive index difference and the incidence angle, is accompanied by transmission losses, deteriorated contrast, and veil glare. The additive energy loss further brings about ghost images because several components are involved in an optical system.³ To reduce the intensity of reflection and to eliminate the resultant detrimental effects, a variety of index-matching materials have been utilized to render light destructive interferences in numerous optical applications.^{4–8} However, most quarter wavelength single-layer antireflection coatings suffer from the rare selection of low refractive index materials, high fabrication cost, and narrowband antireflection performance. Although multilayer antireflection coatings have been extensively explored to suppress the reflection in a large wavelength range, poor optical and thermal stability resulting from mismatched thermal expansion coefficients between foreign materials are clearly evident.^{9,10} Hence, such approaches are not well suited for developing large areal and long-term antireflection coatings.

Natural surface architectures have provided multitudinous distinct functionalities to deal with survival challenges over four billion years of revolution.¹¹ Taking nature as a source of bio-inspiration, the booming of research centered on biomimicking the natural architectures has witnessed striking developments in advanced structures, materials, and applications.^{12–18} For instance, corneal lenses of moth compound

eyes are covered with nipple-like protuberances, typically of subwavelength spacing and height.¹⁹ The hexagonally nonclose-packed nipple arrays establish a graded refractive index transition, eliminating broadband optical reflection. Similar nonclose-packed structure arrays can also be found on cicada wings, glasswing butterfly wings, and dragonfly wings for minimizing the light reflection and light scattering to avoid being tracked during flight.^{20–23} Inspired by the broadband antireflective properties of insects, periodic arrays of subwavelength structures with high aspect ratios, including pillar arrays, cone arrays, wire arrays, and pyramid arrays, have been engineered as antireflective structures by extensive top-down lithography-based fabrication methodologies.^{24–29} Nevertheless, current top-down methodologies require sophisticated facilities and are costly to implement. In addition, most lithographic technologies suffer from low resolution for fabricating subwavelength features. Other than lithographic technology, electroless metal nanoparticle-assisted catalytic etchings have been developed to realize large surface area hierarchical structures.^{30–32} Although texturing nanoscale pits on microstructured surfaces is identified to provide antireflective properties, the fabrication involves either a multistep process or a long etching duration. Besides that, the irregular

Received: March 5, 2020

Revised: April 23, 2020

Published: April 24, 2020



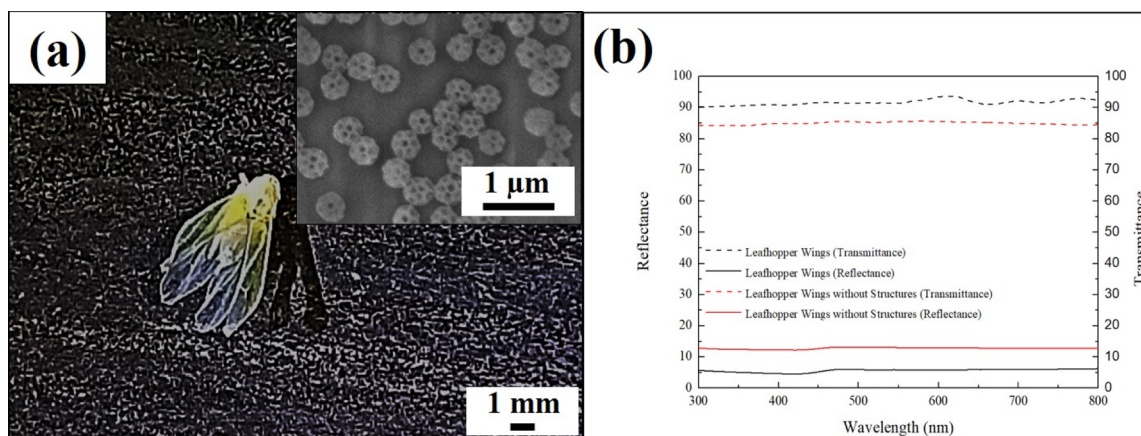


Figure 1. (a) Photographic image of a leafhopper. The insert shows a top-view SEM image of the leafhopper wing. (b). Optical reflectance and optical transmittance spectra obtained from the leafhopper wings before/after erasing the integumentary brochosomes at normal incidence.

arrangement of structures offers poor light management. Contrarily, bottom-up self-assembly methodologies provide an inexpensive and high throughput alternative in developing periodic subwavelength features.³³ Unfortunately, the as-fabricated periodic arrays of subwavelength antireflective structures, such as domes, holes, spheres, and so on, are limited by low aspect ratios, and thence cannot suppress optical reflection at large incidence angles.^{34–37}

Unlike many other insects, leafhoppers, inhabiting forests, grasslands, and agricultural fields throughout the world, actively coat their wings with a monolayer of nonsticky proteinaceous secretory particles, named brochosomes.^{38,39} Even though the leafhopper-produced embroidered ball-like integumentary brochosomes are with relatively low aspect ratios, the hierarchical structures generate smooth and low refractive index gradients in wide incidence angles. As a result, the brochosomal coating exhibits broadband omnidirectional antireflection behavior, and functions as a camouflage layer to protect themselves.⁴⁰ Inspired by the leafhopper-produced brochosomes, this research combines a scalable self-assembly technology and a simple colloidal templating methodology to develop a nonlithographic approach enabling the fabrication of periodic embroidered ball-like antireflective structures. The surface morphologies of the as-fabricated hierarchical structure arrays can be well controlled for systematically investigating the dependence of structural geometry on omnidirectional antireflection performance.

EXPERIMENTAL METHODS

Materials and Reagents. The leafhopper, which had been selected as a biomimetic prototype, was acquired from Flying Insect Specimen Studio. The chemicals used for the synthesis of silica colloids included anhydrous ethanol (99.5%), aqueous ammonium hydroxide (28%), tetraethyl orthosilicate (98%), and ultrapure water (18.4 MΩ cm). Anhydrous ethanol, aqueous ammonium hydroxide, and tetraethyl orthosilicate were provided by Sigma-Aldrich Corporation and used without further treatment. Ultrapure water was collected from a Milli-Q IQ 7000 purification system. The UV-curable ethoxylated trimethylolpropane triacrylate (ETPTA) monomer (SR 454, 98%), the ethylene glycol diacrylate (EGDA) monomer (90%), and the photoinitiator, 2-hydroxy-2-methyl-1-phenyl-1-propanone (Darocur 1173, 96%), were collected from Sartomer, Sigma-Aldrich Corporation, and BASF Corporation, respectively. Poly(urethane acrylate) (PUA) (ETERANE 89,452, 22,000 g/mol) was purchased from Eternal Materials Company Limited. N-Type silicon wafers were acquired from The Semiconductor Materials and

Logistics Network, while the silicon wafer primer, 3-acryloxypropyl trichlorosilane (APTCS, 98%), was obtained from Gelest, Inc.

Preparation of Spherical Silica Colloidal Suspensions. Narrowly size-distributed silica colloids with varied diameters were synthesized using a standard StÖber method.⁴¹ The StÖber silica colloids were collected and purified in anhydrous ethanol by applying five centrifugation–redispersion cycles to eliminate aqueous ammonium hydroxide and any unreacted silanes. The purified silica colloids were then dispersed in anhydrous ethanol, of which the silica colloid volume fraction was adjusted to 1 vol %.

Spin-Coating of Monolayer Nonclose-Packed Colloidal Crystals. After centrifugation of the as-prepared suspension, silica colloids were redispersed in a mixture of ETPTA monomer and photoinitiator (1 vol %), in which the colloid volume fraction was adjusted to 25 vol %. The silica mixture was then deposited on an APTCS-primed silicon wafer. The silicon wafer was tilted to spread the mixture and spun at 500 rpm for 100 s, 2000 rpm for 50 s, 4000 rpm for 30 s, 2500 rpm for 30 s, and 8000 rpm for 120 s. After spin-coating, the ETPTA monomer was photopolymerized in an X Lite 500 Pulsed UV curing chamber for 10 s to fabricate a monolayer of silica colloidal crystals.

Fabrication of Nonclose-Packed Embroidered Ball-Like Structure Arrays. A commercial PUA solution (20 vol %) was poured onto the colloidal crystals. After being dried under ambient conditions, the PUA hole array was created and removed from the silicon wafer gently. The PUA film was then immersed in the as-prepared silica colloidal suspension, followed by spinning at 500 rpm to deposit silica colloids on the holes. Subsequently, a mixture of EGDA monomer and photoinitiator was cast onto the silica colloid-attached PUA film and degassed in a vacuum chamber for 20 min. After UV polymerization of the EGDA monomer, the PEGDA film was peeled off, and the silica colloids were selectively removed using a hydrofluoric acid aqueous solution (2 vol %) to engineer nonclose-packed embroidered ball-like structure arrays.

Characterization. Photographic images of a leafhopper and leafhopper-inspired structure-coated substrates were acquired with a Canon SX 740 HS digital camera. A JEOL 6335F field-emission scanning electron microscope was employed to characterize the surface morphologies and structures of the samples, on which extremely thin platinum layers were sputter-deposited before imaging. The reflectance spectra and transmittance spectra of the samples in the wavelength range of 250–800 nm were obtained using an Ocean Optics HR4000 fiber-optic spectrometer with a tungsten-halogen light source. A standard silicon wafer was used for calibration.

RESULTS AND DISCUSSION

In this research, a leafhopper (*Thaia rubiginosa*, Motschulsky) is selected as a biomimetic prototype to engineer antireflective structures. The leafhopper wings, as displayed in Figure 1a, are

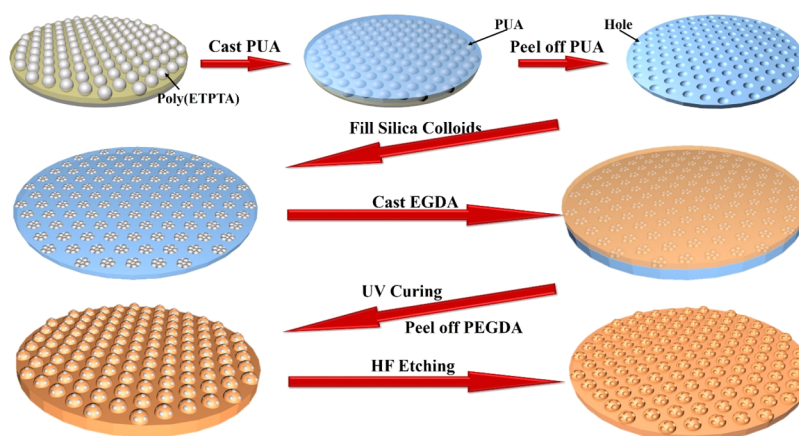


Figure 2. Schematic illustration of the biomimetic procedures for engineering the leafhopper wing-inspired antireflection coating.

highly transparent in appearance under white light illumination, which provide camouflage against predators. The transparency originates from leafhopper-produced integumentary brochosomes (insert of Figure 1a), which are embroidered ball-like submicrometer-scale particles covered with nanometer-scale holes. The brochosomal coating builds a gradual refractive index transition to reduce incident light reflection, and therefore results in a broadband antireflection performance. As shown in Figure 1b, the average reflectance and the average transmittance of the leafhopper wings in the visible wavelength range of 380–740 nm are ca. 5, and 91%, respectively. It is worth mentioning that the average reflectance is increased by ca. 7%, while the average transmittance is decreased by ca. 7% after erasing the non-stick brochosomes on leafhopper wings. This further demonstrates that the embroidered ball-shaped architecture can yield the broadband antireflective function.

Inspired by the leafhopper-produced integumentary brochosomes, embroidered ball-like structure arrays are engineered by integrating the bottom-up self-assembly technology and soft lithography technique. In the biomimetic procedure (Figure 2), monolayered nonclose-packed 250 nm silica colloidal crystals are self-assembled on a silicon wafer using spin-coating technology, followed by casting a PUA solution to create a nonclose-packed 250 nm hole array. Under visible light illumination, both of silicon wafer and the PUA film display characteristic six-arm diffraction patterns (Figure 3), which are identical to long-range nonclose-packed structures.^{42,43} The crystal lattices are further evident in the inserts of Figure 3. Even though a few defects can be found, the hexagonal

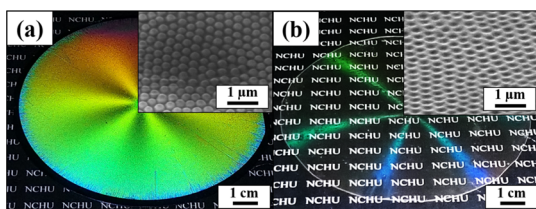


Figure 3. (a) Photographic image of nonclose-packed 250 nm silica colloidal crystals on a silicon wafer prepared by the spin-coating technology. The insert shows a top-view SEM image of the wafer. (b) Photographic image of a PUA film with nonclose-packed 250 nm holes templated from the wafer in (a). The insert shows a top-view SEM image of the film.

arrangements of nonclose-packed structures are clearly identified. The as-fabricated PUA film is immersed in a 90 nm silica colloidal suspension (1 vol %), followed by a spinning process to remove excess silica colloids until the holes are filled with silica colloids (Figure 4a). The silica colloids in

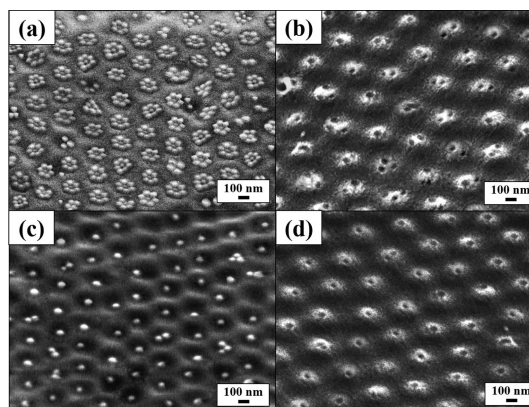


Figure 4. (a) Top-view SEM image of nonclose-packed 250 nm holes filled with 90 nm silica colloids. (b) Top-view SEM image of embroidered ball-like hierarchical structures templated from the holes in (a). (c) Top-view SEM image of nonclose-packed 250 nm holes with 90 nm silica colloids attached. (d) Top-view SEM image of hierarchical structures templated from the holes in (c).

each hemispherical hole tend to be in physical contact with each other, which is attributed to the attractive capillary forces between the colloids. Subsequently, the silica colloid-attached hole array is exploited as a second-generation template on which a mixture of EGDA monomer and photoinitiator is poured over, and degassed in a vacuum environment to remove any trapped air. After UV polymerization of the EGDA monomer, the silica colloid-embedded PEGDA film can be peeled off easily. The embedded silica colloids are finally wet-etched to engineer leafhopper wing-inspired embroidered ball-like structure arrays. As shown in Figure 4b, the nonclose-packed arrangement and hexagonal ordering can be well reserved in the biomimetic procedure. Additionally, the average height of the hierarchical structures is about 125 nm. In comparison with the surface morphology of the bumps templated from the nonclose-packed featureless hole array (Figure S1), it is evident that nanometer-scale holes are created on the hierarchical structures. It is worth mentioning

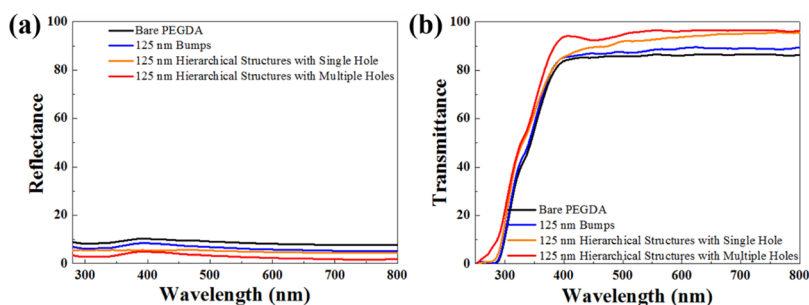


Figure 5. (a) Normal incidence optical reflectance spectra and (b) normal incidence optical transmittance spectra acquired from a bare PEGDA substrate and PEGDA substrates coated with bump arrays and embroidered ball-like hierarchical structure arrays. The structures are with an average height of ca. 125 nm.

that the surface morphologies and the sizes of the embroidered ball-like structures can be easily adjusted by introducing silica colloids of different sizes. Interestingly, the spinning process duration can be extended until only one single silica colloid can be retained in each hole (Figure 4c). Afterward, the single silica colloid-attached hole array can serve as a template to fabricate nonclose-packed single-hole covered hierarchical structure array (Figure 4d).

As mentioned previously, hierarchical structures are capable of developing a gradual refractive index transition at the air/substrate interface to efficiently reduce optical reflection. To investigate the antireflection functionality of the embroidered ball-like hierarchical structure arrays shown in Figure 4, the normal incidence optical reflectance spectra and transmittance spectra of a featureless PEGDA substrate, a bump array-coated PEGDA substrate, and embroidered ball-like hierarchical structure array-coated PEGDA substrates are evaluated and compared in Figure 5. It is worth noting that the tungsten-halogen light source for spectroscopy features weak emission in the wavelength range below 380 nm, resulting in the low reflectance and low transmittance in the wavelength range from 250 to 380 nm. The average optical reflectance in the visible spectral range is reduced from ca. 9% for a bare substrate to ca. 7% for a bump array-coated substrate. Compared with that, the optical reflectance is further reduced by introducing hierarchical structure arrays. The average reflectance of multiple hole-covered embroidered ball-like hierarchical structure array-coated substrate reaches ca. 4% over the whole visible spectrum, while the average transmittance of 94% is achieved, revealing broadband antireflection functionality. The antireflection functionality can be further comprehended by comparing the calculated effective refractive index changes in the templated structures.^{44,45} A hemispherical bump-shaped profile displayed in Figure 6 is adopted to modulate the structures, which are divided into multiple layers. The effective refractive index of each layer can then be simulated using the effective medium theory. As revealed in Figure 6, it is apparent that the construction of more nanometer-scale holes in the hierarchical structures leads to a lower optical reflectance and a higher optical transmittance, which resulted from the lower average refractive index and the smoother refractive index gradient across the hierarchical structures. Moreover, the simulated normal incidence reflectance and transmittance of the nonclose-packed embroidered ball-like hierarchical structure array produced by a regular coupled-wave analysis model agree well with the experimental results (Figure S2), further confirming the effect of the hierarchical structure on the antireflection performance.

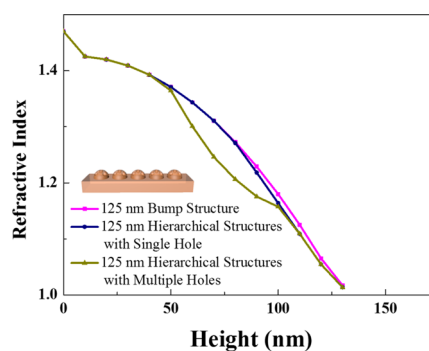


Figure 6. Comparison of the change in the calculated effective refractive index from the PEGDA substrate (height = 0) to the top of templated bumps and embroidered ball-like hierarchical structures. The structures are with an average height of ca. 125 nm.

To better understand the embroidered ball-like hierarchical structure-shape effect on the antireflection capability, the optical reflectance spectra and optical transmittance spectra of all the substrates mentioned above are measured at various incidence angles from 30, 45, and 60 to 75° (Figure S3). The results in the visible wavelength range of 380–740 nm are further averaged and summarized in Figure 7. As revealed in Figure 7a, although all the optical reflectances increase with increasing incidence angle, the average optical reflection can be suppressed by 5% at 0° and 19% at 75° as a multiple hole-covered embroidered ball-like hierarchical structure array is sculpted on the substrate. In contrast, the average transmittances of all the substrates decrease with increasing incidence angles. Importantly, the average transmittance of the multiple hole-covered embroidered ball-like hierarchical structure array-coated substrate is significantly improved even for large incidence angles, and an average transmittance of 60% can be reached at 75°. It is noteworthy that diffuse reflection occurs as the incident light interacts within the periodic structures, where the interstructure distance and the structure size are comparable with the light wavelength. As a result, the incident light is partially refracted or reflected in random directions after a few internal reflections. This suggests that the diffuse reflection losses at various incidence angles can be reduced by introducing subwavelength hierarchical structures, which possess smooth refractive index gradients in wide incidence angles (Figure S4). Therefore, the propagation of light is guided by the effective refractive index transition from air to the substrate. The omnidirectional antireflection capability can be interpreted by mapping the calculated effective refractive index across the hierarchical structures at

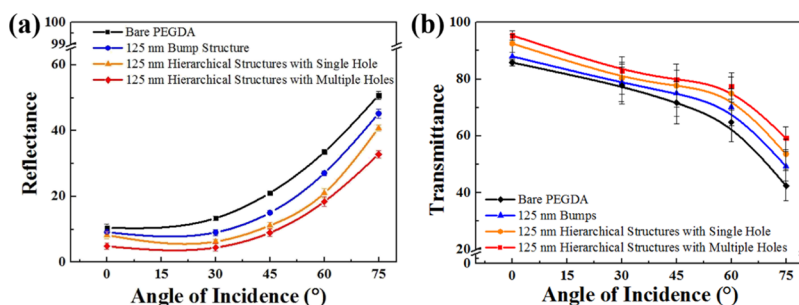


Figure 7. (a) Optical reflectance spectra and (b) optical transmittance spectra at various incidence angles acquired from a bare PEGDA substrate and PEGDA substrates coated with bump arrays and embroidered ball-like hierarchical structure arrays. The structures are with an average height of ca. 125 nm.

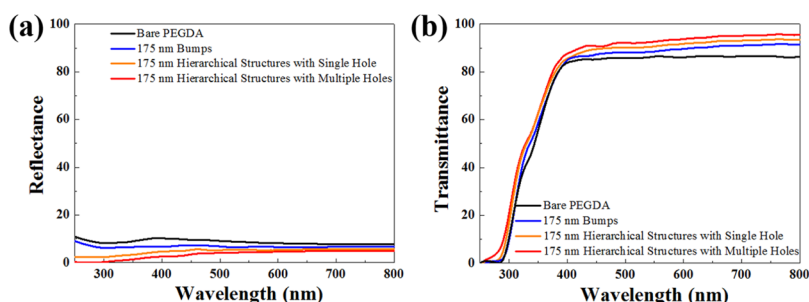


Figure 8. (a) Normal incidence optical reflectance spectra and (b) normal incidence optical transmittance spectra acquired from a bare PEGDA substrate and PEGDA substrates coated with bump arrays and embroidered ball-like hierarchical structure arrays. The structures are with an average height of ca. 175 nm.

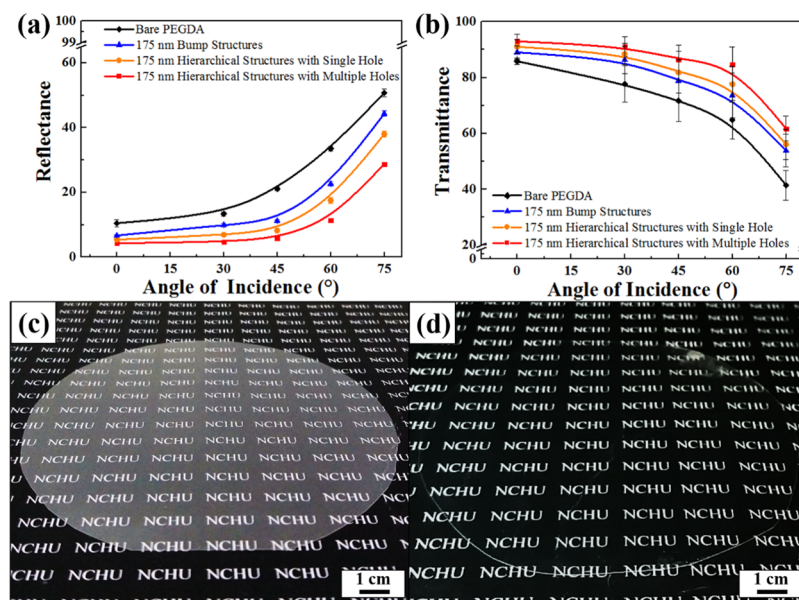


Figure 9. (a) Optical reflectance spectra and (b) optical transmittance spectra at various incidence angles acquired from a bare PEGDA substrate and PEGDA substrates coated with bump arrays and embroidered ball-like hierarchical structure arrays. The structures are with an average height of ca. 175 nm. Photographic images of (c) a bare PEGDA substrate and (d) a PEGDA substrate coated with embroidered ball-like hierarchical structure arrays at a 75° incident angle.

30, 45, and 60 and 75°. As shown in Figure S4, the multiple hole-covered embroidered ball-like hierarchical structure array possesses the lowest effective refractive index and the smoothest refractive index gradient among the substrates, and therefore possesses optimum antireflection capability.

To further generate a smoother refractive index transition, nonclose-packed 350 nm silica colloidal crystals are self-assembled and utilized as a template to fabricate a nonclose-

packed 350 nm hole array (Figure S5). The hole array then served as a second-generation template for engineering a multiple 90 nm hole-covered embroidered ball-like hierarchical structure array, a single 90 nm hole-covered embroidered ball-like hierarchical structure array, and a bump array following the biomimetic procedure as mentioned previously (Figures S6 and S7). The structures have an average height of ca. 175 nm and are hexagonally nonclose-packed. Interestingly, in

comparison with the optical spectra of the structures templated from 250 nm hole arrays, the structures templated from 350 nm hole arrays display a lower optical reflectance and a higher optical transmittance at normal incidence (Figures S8 and 8). The average normal incidence reflectance of the multiple hole-covered embroidered ball-like hierarchical structure (175 nm in height) array-coated substrate reaches 3%, while the average normal incidence transmittance of that can achieve 96%. It is noted that the optical reflectances and optical transmittances of the above substrates exhibit similar tendencies at various incidence angles (Figure S9). Most importantly, although the antireflective property is still sensitive to the incidence angle, the multiple hole-covered embroidered ball-like hierarchical structure array-coated substrate array displays an average reflectance of 28% and an average transmittance of 63% even at 75° (Figure 9a,b). Owing to the smoother refractive index transition and the lower average calculated refractive index (Figures 10 and S10), less incident visible light is reflected

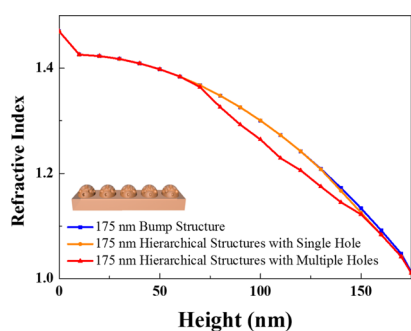


Figure 10. Comparison of the change of the calculated effective refractive index from the PEGDA substrate (height = 0) to the top of templated bumps and embroidered ball-like hierarchical structures. The structures are with an average height of ca. 175 nm.

from the hierarchical structures templated from 350 nm holes, and therefore results in an improved broadband omnidirectional antireflection performance (Figure 9c,d).

CONCLUSIONS

To conclude, we have developed a scalable nonlithographic approach for engineering nonclose-packed embroidered ball-like hierarchical structure arrays, inspired by the brochosomal coatings on leafhopper wings. Optical measurements disclose that the bioinspired structure arrays feature broadband omnidirectional antireflection capability. Additionally, higher hierarchical structures possess a smoother refractive index transition, and exhibit an improved antireflection performance. The antireflection coating holds promise for various technological applications in optical devices.

ASSOCIATED CONTENT

Supporting Information

The Supporting Information is available free of charge at <https://pubs.acs.org/doi/10.1021/acs.langmuir.0c00634>.

Photographic images, SEM images, calculated effective refractive index transitions, optical reflectance spectra, and optical transmittance spectra of the as-engineered colloidal crystals, bump arrays, and embroidered ball-like hierarchical structure arrays (PDF)

AUTHOR INFORMATION

Corresponding Author

Hongta Yang – Department of Chemical Engineering, National Chung Hsing University, Taichung 40227, Taiwan;
 orcid.org/0000-0002-5822-1469; Email: hyang@dragon.nchu.edu.tw

Authors

Chih-Wei Lei – Department of Chemical Engineering, National Chung Hsing University, Taichung 40227, Taiwan
 Ru-Yu Chen – Department of Chemical Engineering, National Chung Hsing University, Taichung 40227, Taiwan

Complete contact information is available at:
<https://pubs.acs.org/doi/10.1021/acs.langmuir.0c00634>

Notes

The authors declare no competing financial interest.

ACKNOWLEDGMENTS

The research was supported by the National Science Council under grant numbers MOST 108-2221-E-005-040 and MOST 108-2221-E-005-038-MY2.

REFERENCES

- Buskens, P.; Burghoorn, M.; Mourad, M. C. D.; Vroon, Z. Antireflective Coatings for Glass and Transparent Polymers. *Langmuir* **2016**, *32*, 6781–6793.
- Ye, X.; Shao, T.; Sun, L.; Wu, J.; Wang, F.; He, J.; Jiang, X.; Wu, W.-D.; Zheng, W. Plasma-Induced, Self-Masking, One-Step Approach to an Ultrabroadband Antireflective and Superhydrophilic Subwavelength Nanostructured Fused Silica Surface. *ACS Appl. Mater. Interfaces* **2018**, *10*, 13851–13859.
- Tsai, T.-Y.; Lee, Z.-C.; Tsao, H.-X.; Lin, S.-T. Minimization of Fresnel Reflection by Anti-Reflection Fiber Bragg Grating Inscribed at the Fiber Ends. *Opt. Express* **2019**, *27*, 11510–11515.
- Bacon-Brown, D. A.; Braun, P. V. Tunable Antireflection Coating to Remove Index-Matching Requirement for Interference Lithography. *Adv. Opt. Mater.* **2018**, *6*, 1701049.
- Tadepalli, S.; Slocik, J. M.; Gupta, M. K.; Naik, R. R.; Singamaneni, S. Bio-Optics and Bio-Inspired Optical Materials. *Chem. Rev.* **2017**, *117*, 12705–12763.
- Alshomrany, A. S.; Nguyen, Z.; MacLennan, J. E.; Clark, N. A. Scanned Conical Illumination as a Probe of Electro-Optic Retro-Reflection. *Opt. Express* **2019**, *27*, 18383–18398.
- Mariani, S.; Robbiano, V.; Iglío, R.; La Mattina, A. A.; Nadimi, P.; Wang, J.; Kim, B.; Kumeria, T.; Sailor, M. J.; Barillaro, G. Moldless Printing of Silicone Lenses with Embedded Nanostructured Optical Filters. *Adv. Funct. Mater.* **2020**, *30*, 1906836.
- Wang, F.; Manjare, M.; Lemasters, R.; Li, C.; Harutyunyan, H. Enhancing Second-Harmonic Generation Using Dipolar-Parity Modes in Non-Planar Plasmonic Nanocavities. *Opt. Lett.* **2019**, *44*, 2787–2790.
- Han, Z. W.; Wang, Z.; Feng, X. M.; Li, B.; Mu, Z. Z.; Zhang, J. Q.; Niu, S. C.; Ren, L. Q. Antireflective Surface Inspired from Biology: a Review. *Biosurf. Biotribol.* **2016**, *2*, 137–150.
- Kitamura, S.; Kanno, Y.; Watanabe, M.; Takahashi, M.; Kuroda, K.; Miyata, H. Films with Tunable Graded Refractive Index Consisting of Spontaneously Formed Mesoporous Silica Nanopinnacles. *ACS Photonics* **2014**, *1*, 47–52.
- Liu, X.; Liang, Y.; Zhou, F.; Liu, W. Extreme Wettability and Tunable Adhesion: Biomimicking beyond Nature? *Soft Matter* **2012**, *8*, 2070–2086.
- Koch, K.; Bhushan, B.; Jung, Y. C.; Barthlott, W. Fabrication of Artificial Lotus Leaves and Significance of Hierarchical Structure for Superhydrophobicity and Low Adhesion. *Soft Matter* **2009**, *5*, 1386–1393.

- (13) Liu, C. Rapid Fabrication of Microfluidic Chip with Three-Dimensional Structures using Natural Lotus Leaf Template. *Microfluid. Nanofluidics* **2010**, *9*, 923–931.
- (14) Lee, S.-M.; Kwon, T. H. Effects of Intrinsic Hydrophobicity on Wettability of Polymer Replicas of a Superhydrophobic Lotus Leaf. *J. Micromech. Microeng* **2007**, *17*, 687–692.
- (15) Jiang, L.; Zhao, Y.; Zhai, J. A Lotus-Leaf-like Superhydrophobic Surface: A Porous Microsphere/Nanofiber Composite Film Prepared by Electrohydrodynamics. *Angew. Chem.* **2004**, *116*, 4438–4441.
- (16) Xi, W.; Qiao, Z.; Zhu, C.; Jia, A.; Li, M. The Preparation of Lotus-Like Super-Hydrophobic Copper Surfaces by Electroplating. *Appl. Surf. Sci.* **2009**, *255*, 4836–4839.
- (17) Bindra, H. S.; Kiran Kumar, A. B. V.; Nayak, R. Optical Properties of a Biomimetically Prepared Hierarchical Structured Polydimethyl Siloxane Template for Potential Application in Anti-Reflection and Photovoltaic Encapsulation. *Mater. Res. Express* **2017**, *4*, 055501.
- (18) Guo, R.; Yu, Y.; Zeng, J.; Liu, X.; Zhou, X.; Niu, L.; Gao, T.; Li, K.; Yang, Y.; Zhou, F.; Zheng, Z. Biomimicking Topographic Elastomeric Petals (E-Petals) for Omnidirectional Stretchable and Printable Electronics. *Adv. Sci.* **2015**, *2*, 1400021.
- (19) Siddique, R. H.; Gomard, G.; Hölscher, H. The Role of Random Nanostructures for the Omnidirectional Anti-Reflection Properties of the Glasswing Butterfly. *Nat. Commun.* **2015**, *6*, 6909.
- (20) Sun, C.-H.; Gonzalez, A.; Linn, N. C.; Jiang, P.; Jiang, B. Templated Biomimetic Multifunctional Coatings. *Appl. Phys. Lett.* **2008**, *92*, 051107.
- (21) Sun, J.; Bhushan, B. Nanomanufacturing of Bioinspired Surfaces. *Tribol. Int.* **2019**, *129*, 67–74.
- (22) Zhou, H.; Xu, J.; Liu, X.; Zhang, H.; Wang, D.; Chen, Z.; Zhang, D.; Fan, T. Bio-Inspired Photonic Materials: Prototypes and Structural Effect Designs for Applications in Solar Energy Manipulation. *Adv. Funct. Mater.* **2018**, *28*, 1705309.
- (23) Morikawa, J.; Ryu, M.; Seniutinas, G.; Balčytis, A.; Maximova, K.; Wang, X.; Zamengo, M.; Ivanova, E. P. Nanostructured Antireflective and Thermoisolative Cicada Wings. *Langmuir* **2016**, *32*, 4698–4703.
- (24) Sun, J.; Wang, X.; Wu, J.; Jiang, C.; Shen, J.; Cooper, M. A.; Zheng, X.; Liu, Y.; Yang, Z.; Wu, D. Biomimetic Moth-eye Nanofabrication: Enhanced Antireflection with Superior Self-cleaning Characteristic. *Sci. Rep.* **2018**, *8*, 5438.
- (25) Chen, Y.-C.; Huang, Z.-S.; Yang, H. Cicada-Wing-Inspired Self-Cleaning Antireflection Coatings on Polymer Substrates. *ACS Appl. Mater. Interfaces* **2015**, *7*, 25495–25505.
- (26) Chien, C.-Y.; Chen, Y.-H.; Chen, R.-Y.; Yang, H. Dragonfly-Wing-Inspired Inclined Irregular Conical Structures for Broadband Omnidirectional Antireflection Coatings. *ACS Appl. Nano Mater.* **2020**, *3*, 789–796.
- (27) Kraus, M.; Diao, Z.; Weishaupt, K.; Spatz, J. P.; Täschner, K.; Bartsch, H.; Schmittgens, R.; Brunner, R. Combined “Moth-Eye” Structured and Graded Index-Layer Anti-Reflecting Coating for High Index Glasses. *Opt. Express* **2019**, *27*, 34655–34664.
- (28) Ko, D.-H.; Tumbleston, J. R.; Henderson, K. J.; Euliss, L. E.; DeSimone, J. M.; Lopez, R.; Samulski, E. T. Biomimetic Microlens Array with Antireflective “Moth-Eye” Surface. *Soft Matter* **2011**, *7*, 6404–6407.
- (29) Han, Z.; Wang, Z.; Li, B.; Feng, X.; Jiao, Z.; Zhang, J.; Zhao, J.; Niu, S.; Ren, L. Flexible Self-Cleaning Broadband Antireflective Film Inspired by the Transparent Cicada Wings. *ACS Appl. Mater. Interfaces* **2019**, *11*, 17019–17027.
- (30) Bindra, H. S.; R, J.; Kumeria, T.; Nayak, R. Rapid Processing of Wafer-Scale Anti-Reflecting 3D Hierarchical Structures on Silicon and Its Templatation. *Materials* **2018**, *11*, 2586.
- (31) Qi, D.; Lu, N.; Xu, H.; Yang, B.; Huang, C.; Xu, M.; Gao, L.; Wang, Z.; Chi, L. Simple Approach to Wafer-Scale Self-Cleaning Antireflective Silicon Surfaces. *Langmuir* **2009**, *25*, 7769–7772.
- (32) Yeo, C. I.; Song, Y. M.; Jang, S. J.; Lee, Y. T. Wafer-Scale Broadband Antireflective Silicon Fabricated by Metal-Assisted Chemical Etching using Spin-Coating Ag Ink. *Opt. Express* **2011**, *19*, A1109–A1116.
- (33) Gao, P.; He, J.; Zhou, S.; Yang, X.; Li, S.; Sheng, J.; Wang, D.; Yu, T.; Ye, J.; Cui, Y. Large-Area Nanosphere Self-Assembly by a Micro-Propulsive Injection Method for High throughput Periodic Surface Nanotexturing. *Nano Lett.* **2015**, *15*, 4591–4598.
- (34) Kim, J.-G.; Choi, H. J.; Park, K.-C.; Cohen, R. E.; McKinley, G. H.; Barbastathis, G. Multifunctional Inverted Nancone Arrays for Non-Wetting, Self-Cleaning Transparent Surface with High Mechanical Robustness. *Small* **2014**, *10*, 2487–2494.
- (35) Chan, L. W.; Morse, D. E.; Gordon, M. J. Moth Eye-Inspired Anti-Reflective Surfaces for Improved IR Optical Systems & Visible LEDs Fabricated with Colloidal Lithography and Etching. *Bioinspiration Biomimetics* **2018**, *13*, 041001.
- (36) Mokarian-Tabari, P.; Senthamaraiannan, R.; Glynn, C.; Collins, T. W.; Cummins, C.; Nugent, D.; O’Dwyer, C.; Morris, M. A. Large Block Copolymer Self-Assembly for Fabrication of Subwavelength Nanostructures for Applications in Optics. *Nano Lett.* **2017**, *17*, 2973–2978.
- (37) Kuo, W.-K.; Hsu, J.-J.; Nien, C.-K.; Yu, H. H. Moth-Eye-Inspired Biophotonic Surfaces with Antireflective and Hydrophobic Characteristics. *ACS Appl. Mater. Interfaces* **2016**, *8*, 32021–32030.
- (38) Yang, S. K.; Sun, N.; Stogin, B. B.; Wang, J.; Huang, Y.; Wong, T.-S. Ultra-Antireflective Synthetic Brochosomes. *Nat. Commun.* **2017**, *8*, 1285.
- (39) Rakitov, R.; Gorb, S. N. Brochosomes Protect Leafhoppers (Insecta, Hemiptera, Cicadellidae) from Sticky Exudates. *J. R. Soc. Interface* **2013**, *10*, 20130445.
- (40) Ding, Q.; Kang, Y.; Li, W.; Sun, G.; Liu, H.; Li, M.; Ye, Z.; Zhou, M.; Zhou, J.; Yang, S. Bioinspired Brochosomes as Broadband and Omnidirectional Surface-Enhanced Raman Scattering Substrates. *J. Phys. Chem. Lett.* **2019**, *10*, 6484–6491.
- (41) Stöber, W.; Fink, A.; Bohn, E. Controlled Growth of Monodisperse Silica Spheres in the Micron Size Range. *J. Colloid Interface Sci.* **1968**, *26*, 62–69.
- (42) Askar, K.; Phillips, B. M.; Fang, Y.; Choi, B.; Gozubenli, N.; Jiang, P.; Jiang, B. Self-Assembled Self-Cleaning Broadband Antireflection Coatings. *Colloids Surf., A* **2013**, *439*, 84–100.
- (43) Gu, Z.; Kothary, P.; Sun, C.-H.; Gari, A.; Zhang, Y.; Taylor, C.; Jiang, P. Evaporation-Induced Hierarchical Assembly of Rigid Silicon Nanopillars Fabricated by a Scalable Two-Level Colloidal Lithography Approach. *ACS Appl. Mater. Interfaces* **2019**, *11*, 40461–40469.
- (44) Phillips, B. M.; Jiang, P.; Jiang, B. Biomimetic Broadband Antireflection Gratings on Solar-Grade Multicrystalline Silicon Wafers. *Appl. Phys. Lett.* **2011**, *99*, 191103.
- (45) Lin, C.-Y.; Lin, K.-Y.; Tsai, H.-P.; He, Y.-X.; Yang, H. Self-Assembled Dual-Sided Hemispherical Nano-Dimple-Structured Broadband Antireflection Coatings. *Appl. Phys. Lett.* **2016**, *109*, 221601.